5880 *Biochemistry* **2010,** *49,* 5880–5890
DOI: 10.1021/bi100301k

BIOCHEMISTRY
including biophysical chemistry & molecular biology
Article

A Modeled Structure of an Aptamer−gp120 Complex Provides Insight into the Mechanism of HIV-1 Neutralization[†]

Marisa K. Joubert,[‡,#] Nichole Kinsley,[§] Alexio Capovilla,[§,∥] B. Trevor Sewell,[⊥] Mohamed A. Jaffer,[⊥] and Makobetsa Khati*[,‡,@]

[‡]*CSIR Biosciences, P.O. Box 395, Pretoria 0001, South Africa,* [§]*Elevation Biotech, 8 Blackwood Avenue, Parktown, Johannesburg 2193, South Africa,* [∥]*Department of Molecular Medicine and Haematology, Faculty of Health Sciences, University of the Witwatersrand, Johannesburg 2193, South Africa,* [⊥]*Electron Microscope Unit, University of Cape Town, Rondebosch 7701, South Africa, and* [@] *Department of Medicine, Groote Schuur Hospital and University of Cape Town, Cape Town, South Africa*
[#]*Present address: Amgen Inc., One Amgen Center Dr., Thousand Oaks, CA 91320-1799.*

Received March 1, 2010; Revised Manuscript Received May 26, 2010

ABSTRACT: The HIV-1 envelope glycoprotein, gp120, is a key target for a class of drugs called entry inhibitors. Here we used molecular modeling to construct a three-dimensional model of an anti-gp120 RNA aptamer, B40t77, alone and in complex with gp120. An initial model of B40t77 was built from the predicted secondary structure and then subjected to a combination of energy minimization and molecular dynamics. To model the B40t77−gp120 complex, we docked the B40t77 predicted structure onto the CD4-induced epitope of the gp120 crystal structure. A series of gp120 point mutations in the predicted B40t77−gp120 interface were measured for their binding affinity for B40t77 by surface plasmon resonance. According to the model, of the 10 gp120 amino acids that showed a reduction in the level of binding when mutated to alanine, all of them are modeled as making direct contact with B40t77 as part of a hydrogen bonding network. Comparison by electron microscopy of the B40t77−gp120 complex with gp120 alone revealed that only the longest dimension of the complex significantly increased in length, in a manner consistent with the predicted model. Binding assays revealed that B40t77 can weaken the binding of gp120 to the monoclonal antibodies B6, B12, and 2G12, none of which have binding sites that overlap with B40t77, as well as strengthen the binding to the antibody 19b. Thus, B40t77 may induce distant conformational changes in gp120 that disrupt its association with host cells and may suggest a mechanism for aptamer neutralization of HIV-1.

Human immunodeficiency virus type 1 (HIV-1)[1] infection and its associated disease, acquired immunodeficiency syndrome (AIDS), remain significant health problems globally. More than 33 million people are currently estimated to be living with HIV-1 (*1*−*3*). The most dramatic improvement was seen with the introduction of antiviral therapy, which substantially increased the quality and length of life for HIV/AIDS patients. These gains, however, quickly reached a plateau as the genetic diversity of HIV-1 allowed it to evade the immune system and resist antiretrovirals (*4*). Currently, there are more than 800 complete genome sequences in the HIV-1 sequence database (*5*, *6*), an increasing number of which are proving to be drug resistant (*7*). This high degree of variability and complexity has made HIV-1 an extremely challenging target to inhibit (*8*), prompting researchers to explore new avenues for more effective alternatives.

A novel and rapidly growing strategy is the advancement of drugs that inhibit viral entry (*9*). This stage of viral infection is largely attributed to a virion surface glycoprotein called gp120. HIV-1 gp120 is organized into a trimeric spike on the exterior surface of the virion (*10*, *11*) and mediates attachment of the virus to host cells (*12*). The crystal structure of gp120 complexed with the CD4 receptor and a neutralizing antibody revealed specific structural features that suggest a mechanism for immune evasion (*13*). Specifically, the V3 loop of gp120, which is necessary for coreceptor binding and selection, and for interacting with most neutralizing antibodies (*14*), was found to be extended away from the protein in the crystal structure, suggesting that it may act as a "molecular hook" that snags coreceptor binding sites and organizes associations within the viral spike (*15*). The importance of gp120 in HIV-1 entry and pathogenesis has led to the recent pursuit of drugs targeted against it. However, most of these efforts have relied on cellular-based immunity and antibody technology, both of which have failed to produce an effective vaccine or prophylactic reagents for preventing HIV-1 infection.

One of the promising new alternatives to preventing HIV-1 infection and treating infected individuals is the use of aptamer technology (*16*). Aptamers are small nucleic acid molecules that can be designed to bind to and disrupt the function of almost any target molecule (*17*), including biological proteins (*18*). Aptamers offer a range of advantages over other conventional approaches (*19*). Their high affinity and specificity for a specific target give them the recognition properties of antibodies. In addition, their small size and flexibility allow them to fit into clefts where bulkier molecules would otherwise be excluded. In 2006, aptamers achieved a major

[†]This work was supported by the South African Department of Science and Technology (DST) and the Council for Scientific and Industrial Research (CSIR) Parliamentary Grant.

*To whom correspondence should be addressed. Phone: +27128414770. Fax: +2712 8413080. E-mail: Mkhati@csir.co.za.

[1]Abbreviations: AIDS, acquired immunodeficiency syndrome; HIV-1, human immunodeficiency virus type 1; PBMC, peripheral blood mononuclear cells; RU, response units; SPR, surface plasmon resonance.

 Published on Web 06/09/2010

milestone in clinical therapy when an antivascular endothelial growth factor 165 (VEGF165) aptamer called pegaptanib sodium was approved for the treatment of macular degeneration (*20*).

The first aptamers isolated against gp120 bound the protein with high affinity and specificity and neutralized a broad range of HIV-1 clinical isolates (*21*). These RNA aptamers showed the most potent antiviral efficacy of all HIV entry inhibitors described to date (*22*), including antibodies. They suppressed viral replication in cultured human peripheral blood mononuclear cells (PBMC) by up to 1000-fold relative to control cells and neutralized a range of clinical isolates (*21*). While escape mutants and drug resistance are inevitable events (*23*), these aptamers have been shown to penetrate the highly variable exterior surfaces of gp120 to gain access to the conserved core, which the virus cannot afford to mutate without compromising its fitness (*24*). Although the interaction between aptamers and gp120 has been established, to date, almost no structural information about this interaction has been available. Here we have used a structure-based approach to investigate the interaction of gp120 and the 77-nucleotide truncated form of one aptamer, B40t77, shown to have high gp120 binding affinity and neutralization potency (*25*). Using molecular modeling, we generated a three-dimensional structure of the B40t77−gp120 complex and validated the structure by experimental analysis. The results indicate that anti-gp120 aptamers prevent entry of HIV-1 into host cells through steric blocking of the CD4-induced epitope as well as mediating conformational changes that disrupt binding at distant sites.

EXPERIMENTAL PROCEDURES

Aptamer Secondary Structure Prediction. Aptamer secondary structures were predicted using the *mfold* folding algorithm (*26*). A 77-nucleotide truncated from of the B40 aptamer (B40t77), which displayed comparable binding affinity and neutralization potency as the B40 full-length aptamer (*25*), was run through the program, and the lowest-energy conformations were examined further. Secondary structures were adjusted with RNAdraw for presentation (*27*).

Generation of the B40t77−gp120 Model. On the basis of the secondary structures of B40t77 (open and closed), two tertiary models were built using Discovery Studio version 1.7 (Accelrys). First, initial models were built from the primary sequence of B40t77 where nucleotides which were predicted to be base paired according to their secondary structures were specifically matched, but not constrained. Regions of B40t77 with paired residues were treated as double-stranded using standard helix parameters, whereas the rest of the molecule was treated as single-stranded. In both the closed and open forms, nucleotides in the stem region from G1 to C19 were base paired to C77 to G60, in an antiparallel fashion. In the closed form, nucleotides in the loop regions were base paired as follows: A22 to U43, A23 to U42, U26 to G38, G27 to C37, G28 to C36, G29 to C35, C30 to G34, G46 to C57, and C47 to G56. Base pairing in the open form was identical except for A22 to U43, and A23 to U42, which were not paired. These models were placed in a CHARMm force field (*28*) and run through Minimization using the Smart Minimizer Algorithm, for 500 Max Steps, an rms gradient of 0.1, a dielectric constant of 1.0, and no implicit solvent model or shake constraints. The minimized molecules were then run through Solvation using the Explicit Periodic Boundary model, orthorhombic shape, a 55 Å radius centered on the molecule, a minimum distance from boundary of 2 Å, and addition of sodium and chloride counterions. The resulting solvated molecules were run through a Standard Dynamics Cascade which performed several consecutive simulations: Minimization (Steepest Descent algorithm, 500 max steps; Adopted Basis algorithm, 500 max steps), Heating (2000 steps, initial temperature of 50 K, target temperature of 300 K), Equilibration (1000 steps, target temperature of 300 K), and Production (1000 steps, target temperature of 300 K), with no constraints. The B40t77 closed model was then manually docked onto the previously determined gp120 crystal structure [Protein Data Bank (PDB) entry 2B4C] in the approximate binding site as the X5 antibody (*15*). Using interactive features of the program that maximize hydrogen bonding and minimize steric hindrance, the best docked structure was selected. Lastly, interactions in the B40t77−gp120 interface were refined in a final round of minimization using Ligand Minimization with the Smart Minimizer algorithm, 1000 steps, the receptor defined as gp120 and the ligand defined as the 54 nucleotides of B40t77 closest to gp120.

Purification and Refolding of B40t77. The B40t77 DNA template was PCR amplified from the full-length B40 DNA template cloned into the pCR 3.1 cloning vector (Invitrogen) using 5′ and 3′ primers for B40t77 as previously described (*25*). The DNA template was purified by phenol chloroform extraction, precipitation in ethanol, and reconstitution in water. The solution was then run through a Sephadex-G50 column to remove free nucleotides.

For the transcription reaction, 90 μg of B40t77 DNA template was added to a 6 mL transcription mixture consisting of 40 mM Tris-HCl (pH 7.5), 6 mM $MgCl_2$, 1 mM 2′F UTP, 1 mM 2′F CTP (Trilink BioTechnologies), 1 mM ATP, 1 mM GTP (Fermentas), 5 mM DTT, 2 mM spermadine, and 7 units/μL T7 RNA polymerase (Fermentas). The reaction mixture was aliquoted into 200 μL volumes and incubated for 16 h at 37 °C. Two microliters of DNaseI (Fermentas) was added to each 200 μL reaction mixture and the solution incubated for 45 min at 37 °C to stop transcription. The RNA was then purified in the same manner as the DNA template (above). The presence and purity of the RNA transcript were assessed at every stage by electrophoresis on an 11% denaturing (8 M urea) polyacrylamide gel and subsequent visualization with ethidium bromide staining.

Immediately prior to being used, B40t77 was refolded when it was heated at 95 °C for 4 min, cooled at room temperature for 5 min, adjusted to 1× refolding buffer [10 mM HEPES (pH 7.4), 150 mM NaCl, 1 mM $CaCl_2$, 1 mM $MgCl_2$, and 2.7 mM KCl], and cooled for an additional 10 min at room temperature as previously described (*25*).

Native Gel Assessment of B40t77. The following components were run on a 2% agarose gel in the absence of denaturing agents for 1 h at 120 V: the B40t77 PCR amplified product, the B40t77 RNA transcript immediately after refolding, the B40t77 RNA transcript after being frozen at −20 °C overnight, and the Fermentas molecular weight marker (O'generuler ultra low range). Bands were visualized with ethidium bromide staining and UV illumination.

gp120 Protein, Anti-gp120 Monoclonal Antibodies, and CD4 Receptor. The following reagents were obtained through the NIH AIDS Research and Reference Reagent Program, Division of AIDS, NIAID, NIH: HIV-1_{BaL} gp120 from DAIDS, NIAID (catalog no. 4961), HIV-1 gp120 monoclonal antibody B12 (catalog no. 2640), HIV-1 gp120 monoclonal antibody 19b (catalog no. 11436), HIV-1 gp120 monoclonal antibody 17b

(catalog no. 4091), HIV-1 gp120 monoclonal antibody 2G12 (catalog no. 1476), and HIV-1 gp120 monoclonal antibody A32 (catalog no. 11438) (www.aidsreagent.org). HIV-1 gp120 monoclonal antibodies B6 and C11 were kindly donated by L. Morris (National Institute for Communicable Diseases, AIDS Virus Research Unit, Johannesburg, South Africa). The CD4 receptor was obtained from the Sir William Dunn School of Pathology, University of Oxford (Oxford, U.K.).

Mutagenesis and Expression of gp120. Fourteen point mutations were generated in HIV-1_{BaL} gp120 cloned into the pTriEx vector with a C-terminal His_6 tag. Mutagenic primers were designed with the assistance of the Stratagene primer design program (www.stratagene.com/qcprimerdesign) and introduced into gp120 according to the Stratagene site-directed mutagenesis protocol. Briefly, primers were annealed to wild-type gp120 and PCR amplified with Pfu Turbo polymerase (Stratagene) for 16 cycles. Plasmids encoding the gp120 variants were purified using a GeneElute Plasmid purification kit (Sigma-Aldrich, St. Louis, MO), checked by restriction mapping, and sequenced before all transfection experiments. All proteins were expressed in serum-containing medium by transient transfection of HEK293T cells. Briefly, HEK293T cells grown in Dulbecco's modified Eagle's medium containing 10% fetal bovine serum and 1 mM glutamine were seeded at a density of 1.8×10^6 cells per 25 cm^2 tissue culture flask. After overnight incubation, cells were transfected with a mixture containing 20 μg of gp120-expressing plasmid in 62.5 mM $CaCl_2$ and 25 mM HBS. On the following day, the transfection medium was replaced with fresh Dulbecco's modified Eagle's medium containing 2% fetal bovine serum and 1 mM glutamine. After incubation at 37 °C for a further 48 h, culture supernatants were collected and centrifuged at 3500 rpm, to remove cell debris, and stored at −20 °C. Recombinant gp120 expression was verified by SDS−PAGE and Western blotting using a primary anti-gp120 monoclonal antibody (Chessie 13-39.1) and a secondary HRP-conjugated mouse antibody. The expression profiles of all 14 gp120 mutants and the wild type were indistinguishable.

Surface Plasmon Resonance. The affinity and rates of interaction between B40t77 and gp120 were measured on a BIAcore 3000 biosensor instrument using SPR, in a manner similar to that previously described (*29*−*31*). The amounts of protein and aptamer bound were measured as the change in refractive index [recorded in response units (RU)]. All experiments were conducted using HBS-N running buffer [10 mM HEPES (pH 7.4) and 150 mM NaCl] at a flow rate of 5 μL/min, to prevent significant dissociation of the immobilized protein from the chip and to optimize for the fast dissociation rate constant observed (*25*, *32*). For the functional assessment of B40t77 after synthesis and refolding, a CM5 biosensor chip was extensively washed with running buffer and two flow cells were simultaneously monitored. Approximately 19000 RU of HIV-1_{BaL} gp120 was immobilized to flow cell 2, and an equivalent amount of bovine serum albumin (BSA) was immobilized to flow cell 1 as a control flow cell using amine coupling chemistry (*33*). Briefly, gp120 and BSA were coupled to flow cells 2 and 1, respectively, using several steps. (1) EDC and NHS (BIAcore) were mixed in a 1:1 ratio and injected over both flow cells for 10 min. (2) gp120 at 50 μg/mL in 10 mM sodium acetate (pH 5.0) was injected over flow cell 1 for 6 min, followed by injection of BSA over flow cell 2 for 6 min. (3) Ethanolamine (BIAcore) was injected over both flow cells for 10 min to block any remaining activated groups. (4) Glycine-HCl (10 mM, pH 2.5) was injected for 7 min to remove nonspecifically bound protein. Freshly refolded B40t77 (see above) at 500 nM in 1× refolding buffer was then injected over flow cells 1 and 2 for 3 min and allowed to dissociate for 10 min, and the change in RU was recorded. To regenerate the chip, 5 μL of 10 mM NaOH was injected between each run and the RU monitored to make sure that the curves returned to baseline (data not shown), as this had been previously demonstrated not to affect subsequent aptamer binding (*25*, *29*). A flow of running buffer was executed to remove any residual NaOH. Three runs of B40t77 binding to gp120 were performed. The interactive software BIAevaluation version 3.2 was used to subtract the sensogram of the control flow cell from the experimental sensograms.

Kinetic Analysis of Aptamer−*gp120 Mutants*. For the kinetic studies of B40t77 binding to the gp120 mutants, the amount of gp120 on the chip was minimized to avoid saturation and adverse effects. The immobilization was performed essentially as in the SPR section, except that four flow cells were simultaneously monitored, where flow cells 1−3 of the chip were experimental and flow cell 4 was a control. Approximately 8000−10000 RU of the antibody C11 was first immobilized to flow cells 1−3 using amine coupling chemistry, followed by quenching and removal of nonspecifically bound protein. The wild-type and mutant gp120 expressed supernatants were concentrated 20-fold, and then 100 μL was injected one at a time over individual flow cells where the antibody C11 had been bound to capture gp120. As a negative control, an equivalent number of RU of BSA was immobilized to flow cell 4, as described in the SPR section. Ten microliters of the 1:1 mixture of EDC and NHS (BIAcore) was then immediately injected over all flow cells (including the control) to cross-link the bound gp120 to the antibody C11, followed by quenching, removal of nonspecifically bound proteins, and a wash with running buffer. Approximately 1500−3000 RU of gp120 was captured on each chip. Serial dilutions of B40t77 (2000, 1000, 500, 250, 125, and 75 nM) in 1× refolding buffer were made. Fifteen microliters of each B40t77 concentration was injected over flow cells 1−4, and the association and dissociation phases were recorded. The chip was regenerated between each run (as in the SPR section) to make sure that the curves returned to baseline. BIAevaluation version 3.2 was used to process the data. The binding curve from the 1× refolding buffer alone was subtracted for each curve. The association and dissociation data from four to five concentrations per flow cell were fitted simultaneously to a 1:1 binding model with a drifting baseline. The equilibrium dissociation constant (K_d) calculated from two data sets was averaged, where the binding of three concentrations was used for the duplicate set. Error values were calculated as the standard deviation. The dissociation constants and χ^2 values were calculated with the software, and the residuals were examined to ensure the best fit.

Electron Microscopy of gp120 and the B40t77−*gp120 Complex*. HIV-1 gp120 alone and HIV-1 gp120 in complex with B40t77 were prepared for examination by electron microscopy. For the sample of gp120 alone, HIV-1_{BaL} gp120 was prepared at 0.5 mg/mL [86 mM NaCl, 6 mM phosphate, and 1.7 mM KCl (pH 7.4)]. For the B40t77−gp120 sample, 2.5 μL of 0.5 mg/mL B40t77 in 0.1× refolding buffer was added to 10 μL of HIV-1_{BaL} gp120 at 0.5 mg/mL [86 mM NaCl, 6 mM phosphate, and 1.7 mM KCl (pH 7.4)], to give a final ratio of 1 mol of gp120 to 1.1 mol of B40t77, and incubated at room temperature for 30 min. Samples were then shipped overnight to the Electron Microscope Unit at the University of Cape Town.

The two samples, gp120 alone and gp120 in complex with B40t77, were both diluted 1:50 with 20 mM Tris (pH 7.5) and

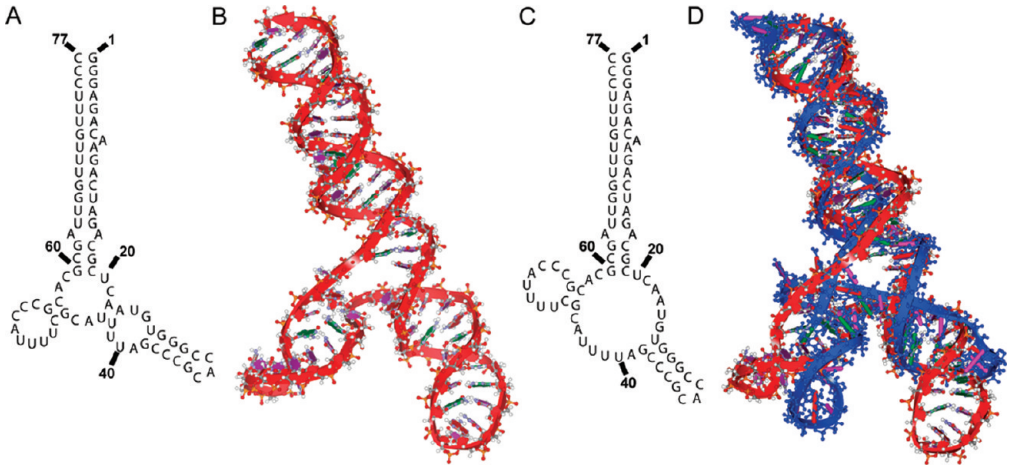

FIGURE 1: Modeled structure of the B40t77 aptamer. (A) Secondary structure prediction of B40t77 showing the closed form of the central loop. (B) Molecular model of the predicted tertiary structure of the closed form of B40t77. (C) Secondary structure of the open form of the central loop. (D) Overlay of the predicted open (blue) and closed (red) tertiary structures of B40t77.

150 mM NaCl. Three microliters of each diluted sample was pipetted onto carbon-coated copper grids that had been made hydrophilic in a glow discharge apparatus (EMS 100 × Glow Discharge). The samples were allowed to adsorb for 30 s. We removed excess solution by blotting with filter paper. The grids were then floated on a drop of water, blotted, and stained with 2% uranyl acetate. Excess stain was removed, and the grids were air-dried. The grids were examined using a LEO 912 TEM operating at 120 kV, and the images were obtained using a 2K × 2K Proscan CCD camera.

Conformational Evaluation of gp120. For the gp120 conformational experiments, immobilization of gp120 was performed as described in the SPR section with the following changes: 50 μg/mL HIV-1_{BaL} gp120 was injected for 3 min, and 13000 RU was immobilized to flow cell 2. Flow cell 1 was used as a blank control. Next, to perform the conformational assays in the absence of aptamer, we injected 15 μL of antibodies (A32, C11, B6, B12, 17b, 19b, and 2G12, 8−50 nM each) or the CD4 receptor (900 nM) in water one at a time over the gp120-immobilized flow cell and control flow cell, and the RU after each injection had been completed was recorded. The binding response at approximately the 700 s time point after the start of injection (60 s after the injected ended) was noted. This time point showed optimal aptamer binding just after the injection was completed, as previously described (*29*). For the conformational studies in the presence of aptamer, 200 nM freshly refolded B40t77 in 1× refolding buffer was injected for 10 min and the change in RU was monitored to ensure binding to gp120. Antibodies or the CD4 receptor was then injected as described above, and the change in RU was recorded. To remove noncovalently bound proteins and thus regenerate the gp120 surface between each subsequent run (in the presence or absence of aptamer), 5 μL of 50 mM NaOH was injected and the RU was monitored to make sure the curves returned to baseline (data not shown). A wash with buffer was performed to remove any residual NaOH. Three trials were performed intermittently, with and without aptamer, and the average and percent uncertainty were calculated as follows:

$$\%\ \text{difference} = [(\text{AVE}\Delta\text{RU with B40t77} \times 100)/(\text{AVE}\Delta\text{RU no B40t77})] - 100$$

$$\%\ \text{uncertainty} = \sqrt{(\text{SD AVE}\Delta\text{RU with B40t77})^2 + (\text{SD AVE}\Delta\text{RU without B40t77})^2}$$

where SD is the standard deviation, AVE is the average value, and ΔRU is the change in response units.

RESULTS

Tertiary Molecular Model of the B40t77 Aptamer. To gain a deeper understanding of aptamer structure in solution, we sought to generate a three-dimensional aptamer model. The B40 aptamer was selected due to the identification of a 77-nucleotide truncated derivative, known as B40t77, which was previously shown to bind gp120 with high affinity and potently neutralize HIV-1 infectivity in close comparison with the full-length B40 (*25*). In addition, preliminary chemical and enzymatic footprinting experiments probing the B40t77 structure had been preformed which provided additional insight into the structure (*25*).

Secondary structure analysis was executed on B40t77 using the *mfold* folding algorithm, and the lowest-energy conformations were examined. Two similar folds were revealed which were consistent with the previously reported secondary structural elements and base pairing of B40t77 (Figure 1) (*25*). The two conformations were identical except for the central ring which was closed in one structure (Figure 1A) and open in the other (Figure 1C), due to the loss of two base pairs, A22 to U43 and A23 to U42. The closed and open secondary structures were used to build two molecular models of B40t77 using Discovery Studio version 1.7. Initial models were constructed from the primary sequence where nucleotides which were predicted to be base paired according to their secondary structures were specifically matched. The resulting model was run though an initial minimization and then placed in a solvated environment with charged ions. A standard dynamics cascade was performed which included several consecutive simulations (minimization, heating, equilibration, and production) to ensure that the lowest-energy state was achieved. Solvating the molecule produced a more energetically favorable structure than the solvent-free form as shown by the more negative potential energy seen after the molecular dynamics simulation was performed, similar to that reported for other RNA modeled structures (*34*). The resulting B40t77 tertiary molecule displays a "Y-like" shape where the stem region is highly base paired and may provide rigidity to the overall molecule (Figure 1B). An overlay of the predicted open and closed tertiary structures revealed that while the stem regions are modeled as virtually superimposable, the branched regions

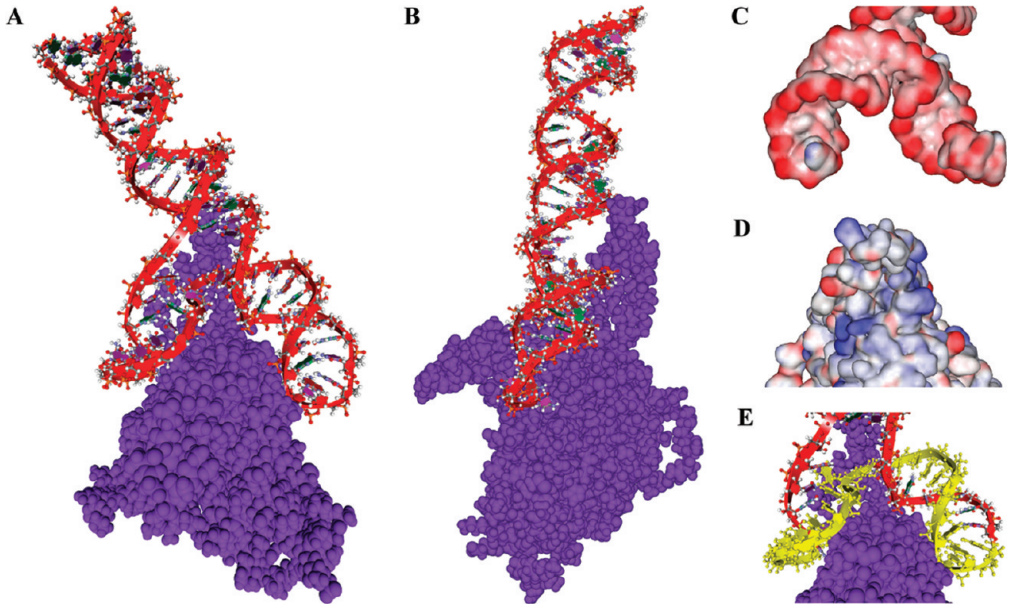

FIGURE 2: Molecular model of the docked B40t77−gp120 complex. (A) The predicted tertiary model of the closed form of the B40t77 aptamer (red) was docked onto the gp120 crystal structure (purple) in the approximate location where the X5 antibody was bound. (B) Side view of the predicted B40t77−gp120 complex. (C) Electrostatic complementarity of the negatively charged phosphate backbone of B40t77 and (D) the positively charged surface of gp120 where it was docked. Negatively charged electrostatic potential is colored red, while positively charged electrostatic potential is colored blue. (E) Of the 24 nucleotides previously predicted to bind gp120, 20 are located directly in the interface of the model (yellow).

showed large conformational differences (Figure 1D). Previous experimental data had identified nucleotides in the branched structure, but not the stem region, as binding to gp120 (*25*).

Three-Dimensional Model of the B40t77−gp120 Complex. A molecular model of the aptamer−gp120 complex was generated to investigate the mechanism of interaction between B40t77 and gp120. We hypothesized that the closed form of B40t77 would be the more likely bound conformation since the only two residues that are base paired in the closed but not open form (A22 to U43 and A23 to U42) also become base paired upon binding gp120 (*25*). The region of B40t77 in the mouth of the Y was targeted, as nucleotides in this region had previously been shown to bind gp120 (*25*). We speculated that the B40t77 binding site and the X5 antibody binding site on gp120 might coincide due to the fact that the X5 antibody was cocrystallized with gp120 on the CCR5 binding site and that partial competition experiments showed that the full-length B40 can compete for binding to the CCR5 binding site with antibodies (*21*), as well as a synthetic peptide of CCR5 (*24*); finally, that alanine scanning mapped the B40t77−gp120 interface to the CCR5 binding site of gp120 (*29*). The predicted structure of the closed form of B40t77 was docked onto the X5 antibody binding site of the gp120 crystal structure (*15*), in a manner that maximized both buried surface area and hydrogen bonding, while minimizing steric clash (Figure 2A,B).

The B40t77−gp120 docked structure is ergonomically suited, electrostatically favorable, and strongly hydrogen bonded. Similar to the X5−gp120 interface, both the binding surfaces of the X5 antibody and the B40t77 phosphate backbone are highly acidic and thus well complemented by the positively charged binding site on gp120 (Figure 2C,D). However, in contrast to the X5−gp120 interface, 10 amino acids of gp120 (Q114, K117, T319, E322, D325, R327, K421, Q422, K432, and R440) are predicted to participate in hydrogen bonding with B40t77, whereas only five participate in binding to the X5 antibody. In our model, of the 24 residues of B40t77 that were previously predicted to bind gp120 (*25*), 16 are modeled to interact directly with gp120, four are modeled as base-paired to an interacting residue, and the remaining four are in the proximity (Figure 2E), showing the agreement of our model with previous footprinting experiments.

Table 1: Binding of B40t77 to HIV-1_{BaL} gp120 Alanine Mutants

gp120[a]	K_d (M)[b]	χ^{2c}	*P* value[d]	effect[e]
wild type	$(2.9 \pm 0.9) \times 10^{-8}$	2.0 ± 1.3	−	/
Q114A	$(2.5 \pm 1.1) \times 10^{-7}$	3.8 ± 0.5	*	↓
K117A	$(6.4 \pm 0.4) \times 10^{-7}$	0.7 ± 0.1	**	↓
K207A	$(3.1 \pm 0.5) \times 10^{-7}$	1.4 ± 1.6	**	↓
E211A	$(6.7 \pm 2.0) \times 10^{-8}$	1.4 ± 1.5	−	/
R298A	$(4.2 \pm 1.6) \times 10^{-7}$	0.5 ± 0.2	*	↓
I307A	$(7.0 \pm 0.1) \times 10^{-9}$	4.1 ± 3.9	*	↑
T319A	$(3.5 \pm 1.1) \times 10^{-7}$	2.4 ± 0.4	*	↓
D325A	$(3.2 \pm 0.6) \times 10^{-4}$	3.3 ± 0.7	**	↓↓↓
R327A	$(3.0 \pm 0.5) \times 10^{-7}$	4.7 ± 0.8	**	↓
K421A	$(1.7 \pm 0.4) \times 10^{-8}$	3.8 ± 3.4	−	/
I423A	$(3.2 \pm 2.6) \times 10^{-8}$	1.5 ± 0.2	−	/
R432A	$(6.3 \pm 2.9) \times 10^{-7}$	1.7 ± 0.1	*	↓
I439A	$(2.9 \pm 0.2) \times 10^{-7}$	1.6 ± 0.1	**	↓
R440A	$(4.0 \pm 0.5) \times 10^{-7}$	0.7 ± 0.1	**	↓

[a]Amino acid numbering is based on the HIV-1 gp120 sequence according to PDB entry 2B4C. [b]K_d represents the equilibrium dissociation constant. Values are averages of duplicate runs, where errors represent the standard deviation. [c]χ^2 is the residual square sum. Averages and standard deviations are shown. [d]*P* values were determined by a *t* test between the K_d values of wild-type and mutant gp120. Statistically significant changes are denoted with one asterisk ($P < 0.05$) and two asterisks ($P < 0.01$). Dashes indicate no significant differences ($P > 0.05$). [e]The effect of B40t77 binding to gp120 mutants as compared to the wild type: /, no change; ↓, ≥10-fold decrease in the level of binding; ↓↓↓, $\geq 10^4$-fold decrease in the level of binding; ↑, increase in the level of binding.

Validation of the B40t77−gp120 Model through Site-Directed Mutagenesis. To investigate the validity of the B40t77−gp120 model in solution, a set of point mutations were designed in the modeled in silico interface. Amino acids of gp120 were targeted that were modeled as externally exposed and

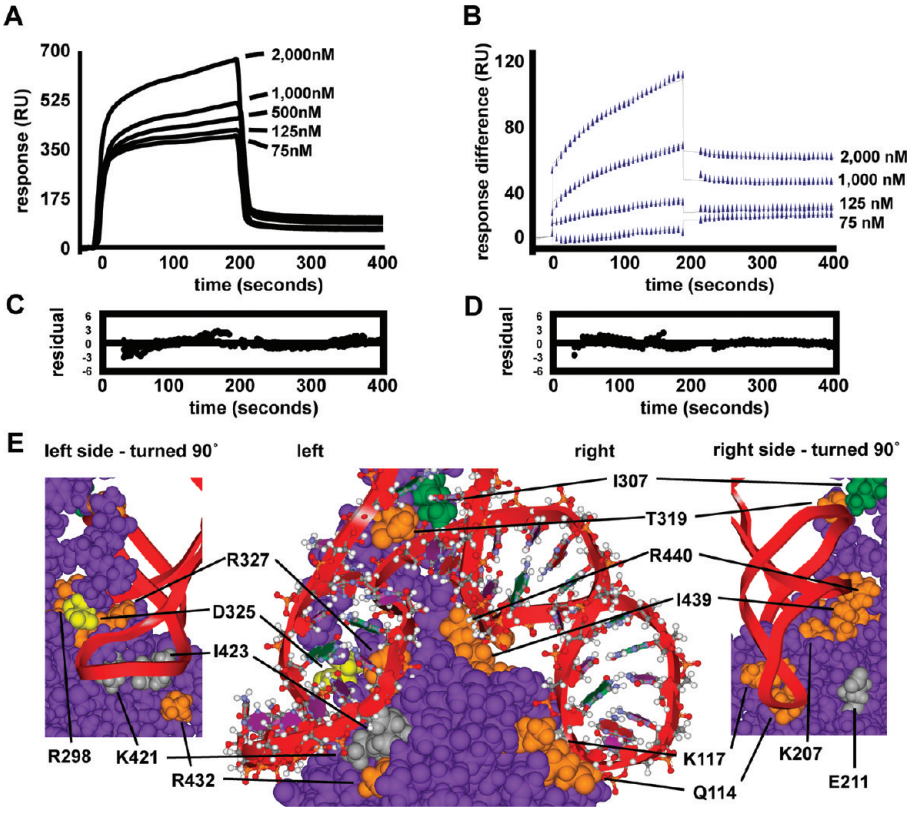

FIGURE 3: Point mutations in the predicted B40t77−gp120 interface disrupt binding. (A) Representative BIAcore sensogram overlay showing binding of B40t77 to the gp120 R440A mutant. Several concentrations of B40t77 were injected over the sensor chip, and the SPR response was recorded as a function of time. (B) Fit of SPR sensograms for gp120 R440A to a 1:1 binding model with a drifting baseline. Experimental sensograms for gp120 R440A are depicted with blue triangles, and the calculated curves are colored black. (C) Representative residual plots of the 1:1 binding model for gp120 K117A and (D) gp120 R440A, shown in panel B. (E) The central panel shows the B40t77−gp120 predicted interface, while the left and right panels depict side views of this interface. The 10 positions that reduced the level of binding when mutated are colored orange (≥10-fold reduction) or yellow (≥10^4-fold reduction). The one that increased the level of binding is colored green, and the three showed no change are colored gray. B40t77 and gp120 are colored red and purple, respectively.

therefore predicted to participate in a stabilizing interaction with B40t77 according to the model. In total, 14 gp120 amino acids were selected and changed, one at a time, to alanine (Table 1). Thirteen were at or near the predicted interface, and one, E211, was selected outside of the interface as a control. To evaluate if the gp120 point mutants were correctly folded, they were tested for their ability to bind the antibody C11. The antibody C11 epitope on gp120 is conformation-dependent, thus controlling for conformational consistency between the various mutants. First, the antibody C11 was immobilized to a CM5 flow cell, and then wild-type gp120 and the mutants were passed one at a time over individual flow cells to determine if the gp120 protein could be captured out of solution. Only gp120 that was correctly folded should be able to bind the antibody C11, as a result of a functional gp120−antibody interface. All 14 gp120 mutants were able to bind to the antibody C11, where more than 1500 RU of all mutants was captured, in a manner equivalent to that of wild-type gp120, demonstrating that the overall integrity of the gp120 mutants had been maintained.

A kinetic assay using SPR technology was used to assess the ability of the gp120 mutants to bind B40t77. Before the kinetic assay was conducted, the B40t77 aptamer was transcribed, purified, and tested for functional integrity by binding to gp120 via SPR (data not shown). After the gp120 wild type and mutants had been captured one at a time by the antibody C11 on separate flow cells (as above), a cross-linker was injected to ensure that gp120 was locked in place. Several concentrations of B40t77 (ranging from 2000 to 75 nM) were passed over each flow cell, and the binding profiles were recorded (Figure 3A). Buffer effects were subtracted, and the resulting curves were fit to a 1:1 model with a drifting baseline (to correct for minor dissociation of the protein from the chip due to inefficient secondary cross-linking) using BIAevaluation (Figure 3B). Wild-type gp120 was found to have a dissociation constant (K_d) of 29 ± 9 nM, in agreement with a K_d of 31 nM reported by other groups (*25*), showing a tight association between B40t77 and gp120. Analysis of residuals showed a random distribution of data points around the *x*-axis as represented in panels C and D of Figure 3. All kinetic data also exhibited a χ^2 value of < 5 showing an acceptable fit of the data to the binding model (Table 1).

The results of kinetic analysis demonstrate that mutating single amino acids in the modeled gp120−B40t77 interface indeed disrupts binding affinity (Table 1). All 14 gp120 mutants were able to bind B40t77, however at different affinities as shown by their altered K_d values. Statistically significant changes in binding, as measured by a *t* test, were seen for gp120 Q114A ($P < 0.05$), K117A ($P < 0.01$), K207A ($P < 0.01$), R298A ($P < 0.05$), I307A ($P < 0.05$), T319A ($P < 0.05$), D325A ($P < 0.01$), R327A ($P < 0.01$), R432A ($P < 0.05$), I439A ($P < 0.01$), and R440A ($P < 0.01$). In summary, nine mutants were found to have K_d values increased by approximately 10-fold, one was found to have a K_d increased $> 10^4$-fold, three showed no change, and one even had a decrease in K_d (Table 1). Upon examination of the gp120−B40t77 modeled structure, we see that all 10 destabilizing mutations make direct contacts with B40t77 in the complex

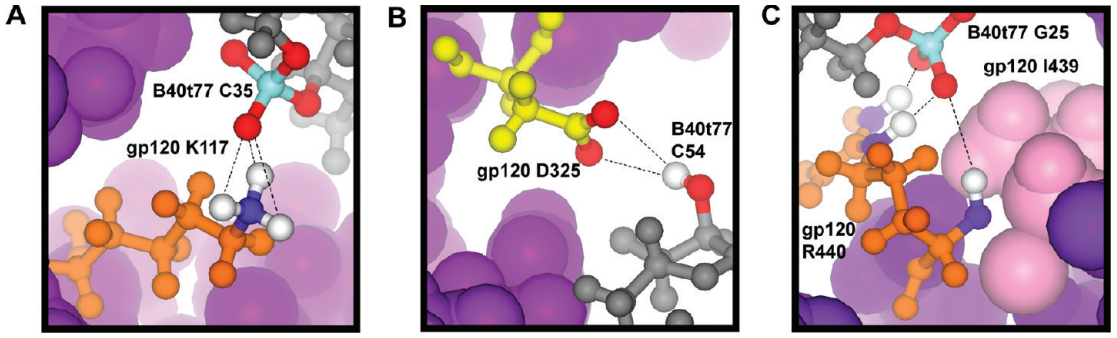

FIGURE 4: B40t77−gp120 docked interface predicted to be stabilized by a network of hydrogen bonds. (A) A close-up of the B40t77−gp120 interface shows that gp120 K117 (orange) was modeled in a position to hydrogen bond to an oxygen atom of B40t77 C35. (B) gp120 D325 (yellow) was placed to hydrogen bond with a hydroxyl group of B40t77 C54. (C) gp120 R440 (orange) was predicted to hydrogen bond with two oxygen atoms of B40t77 G25. I439 (pink), an amino acid adjacent to R440, may disrupt hydrogen bonding through conformational changes. In all panels, gp120 is colored purple and B40t77 gray. Additional atoms of interest are colored white (hydrogen), red (oxygen), dark blue (nitrogen), and light blue (phosphate). Hydrogen bonds are represented by dotted lines.

(Figure 3E), providing a possible explanation for their ability to disrupt association and thus supporting the accuracy of the model. Of the three mutants that showed no change, the first is our noninterface control, E211A. The remaining two, K421A and I423A, are located in the predicted interface. The fact that they did not disrupt binding suggests that they may not contribute substantially to the interaction or that this region of the model is inaccurate. The only activating mutation, I307A, is located in the middle of the V3 loop.

To decipher the primary forces that stabilize the B40t77−gp120 interaction, the modeled interface was examined. Of the 10 gp120 amino acids that weaken binding upon mutation (Table 1), seven (Q114, K117, T319, D325, R327, K432, and R440) are positioned in the model within 2.5 Å of a B40t77 hydrogen bonding partner (Figure 4A−C), two (K207 and R298) are modeled approximately 6 Å from a hydrogen bonding partner, and the remaining one (I439) is modeled next to a hydrogen bond donor (R440) and thus may cause a conformational change that disrupts hydrogen bonding (Figure 4C). Arginine may be the most common amino acid to participate in hydrogen bonding with B40t77 because of its potential to form three hydrogen bonds (Figure 4C), as seen with other aptamer−protein complexes (*35*, *36*). Amino acids of gp120 that are predicted to hydrogen bond appear to donate a hydrogen to B40t77 in all but two cases, E322 and D325 (Figure 4B), where gp120 then becomes the hydrogen bond acceptor. These results suggest that the B40t77−gp120 predicted interface is primarily stabilized by a hydrogen bonding network and electrostatic interactions between charged amino acids of gp120 and the oxygen atoms in the backbone of B40t77.

Electron Microscopy of the B40t77−gp120 Complex. The B40t77−gp120 complex was examined by electron microscopy for comparison to the in silico model. As a preliminary test for electron microscopy, it was determined whether at least a fraction of the aptamer was in the monomeric state and thus could potentially be visualized as a 1:1 complex with gp120, similar to that described for other RNA molecules (*37*). The freshly refolded B40t77 and a sample of B40t77 that had experienced freezing and thawing were run on a native agarose gel to determine if the migration of the molecule was consistent with a mostly monomeric or aggregated state (Figure 5A). The freshly refolded B40t77 migrated on a gel consistent with a monomer and thus might be visualized in solution as a discrete complex with gp120, similar to that predicted by our model. The B40t77

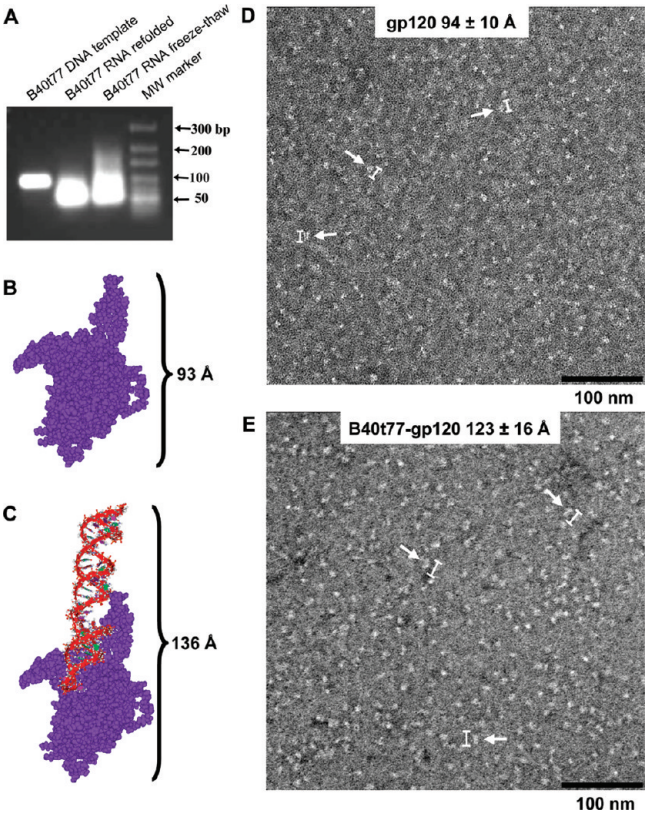

FIGURE 5: Electron microscopy of the B40t77−gp120 complex was in agreement with the model. (A) A native agarose gel shows the migration of the 77-nucleotide refolded B40t77 and B40t77 subjected to freezing and thawing. (B) The longest axis of the gp120 crystal structure is 93 Å. (C) This axis was predicted to increase to 136 Å upon binding B40t77, according to the B40t77−gp120 model. (D) An electron micrograph of gp120 alone contained a homogeneous mixture of particles, where the average longest axis was 94 ± 10 Å. (E) An electron micrograph of the B40t77−gp120 complex revealed that the average longest length increased to 123 ± 16 Å upon formation of the complex. White arrows and bars indicate the longest axis of representative molecules. Error values represent standard deviations of the average values, where differences between the data sets were found to be statistically significant ($P < 0.0001$).

sample that had been subjected to freezing and thawing, however, showed a smearing effect indicating the presence of higher-order multimers (Figure 5A).

Negative stain preparations of gp120 alone and in the presence of B40t77 were visualized by electron microscopy. Both samples

contained a similar mixture of homogeneous particles of approximately the same size (Figure 5). This was not surprising considering that B40t77 is only 23% of the molecular weight of gp120 and thus would not contribute substantially to a change in size. The two samples, however, might differ slightly in the length of their longest axis because of a length contribution from the aptamer while keeping all other dimensions constant (Figure 5B, C). To test this, a set of dimensions were taken from 15 particles from each sample and averaged. All the dimensions between the two samples were relatively constant, except for the longest axis which differed between the two samples. For the gp120 particles, the average length of this axis was determined to be 94 ± 10 Å (Figure 5D), in close agreement with the length of 93 Å calculated from the gp120 crystal structure (Figure 5B). In contrast, the B40t77−gp120 particles had a longer average length of 123 ± 16 Å (Figure 5E), also in agreement with a length of 136 Å predicted from the model (Figure 5C). Differences between these data sets were found to be statistically significant when compared using a *t* test ($P < 0.0001$). This difference in length of nearly 30% of only one dimension between the two samples demonstrates that B40t77 has indeed contributed to an increase in the length of gp120 in a manner that is consistent with our aptamer−gp120 in silico model.

B40t77 Induces Conformational Changes in Distant Binding Sites of gp120. To provide insight into the mechanism of aptamer neutralization of gp120, we investigated the ability of B40t77 to induce conformational changes in gp120 upon binding, as seen with other proteins (*38*, *39*). Antibodies that do not have overlapping binding sites with B40t77 would not be sterically hindered and thus would most likely be inhibited from binding through conformationally induced changes. To test this, the ability of antibodies to bind to gp120 both in the presence and in the absence of B40t77 was measured by SPR. Seven monoclonal antibodies (B6, B12, 17b, C11, A32, 19b, and 2G12) and the CD4 receptor that bind to spatially distinct sites on gp120 were chosen (*40*−*44*), so that conformational changes, and not steric hindrance alone, could be properly assessed (Figure 6A). First, gp120 was immobilized to a CM5 flow cell; then each antibody or the CD4 receptor was injected over the flow cell and allowed to bind, and the RU was recorded. The RU at the 60 s time point after the injection had been completed was noted for further processing. This procedure was performed under two conditions: (1) where B40t77 was first bound to gp120 before antibody binding and (2) in the absence of B40t77. The two values were then compared, and the percent inhibition of antibody binding was calculated (Figure 6B).

Of the eight proteins tested, five were inhibited with respect to binding gp120 by B40t77 (antibodies B6, B12, 17b, and 2G12 and the CD4 receptor), two were uninhibited (antibodies C11 and A32), and one was enhanced (antibody 19b) (Figure 6B). Statistically significant differences in binding were obtained for antibodies B6 ($P < 0.01$), B12 ($P < 0.05$), 17b ($P < 0.05$), 19b ($P < 0.05$), and 2G12 ($P < 0.001$). The CD4 receptor also displayed a reduction in the level of binding; however, the differences were not statistically significant ($P = 0.13$). The ability of B40t77 to inhibit 17b binding by the largest percentage was not surprising because the B40t77 and 17b binding sites are known to overlap, and thus, inhibition is most likely due to steric hindrance caused by the aptamer. However, in contrast, the binding sites of the remaining proteins do not overlap with B40t77, and thus, a reduction in the level of binding is most likely due to a conformational change in gp120 caused by B40t77. The enhanced

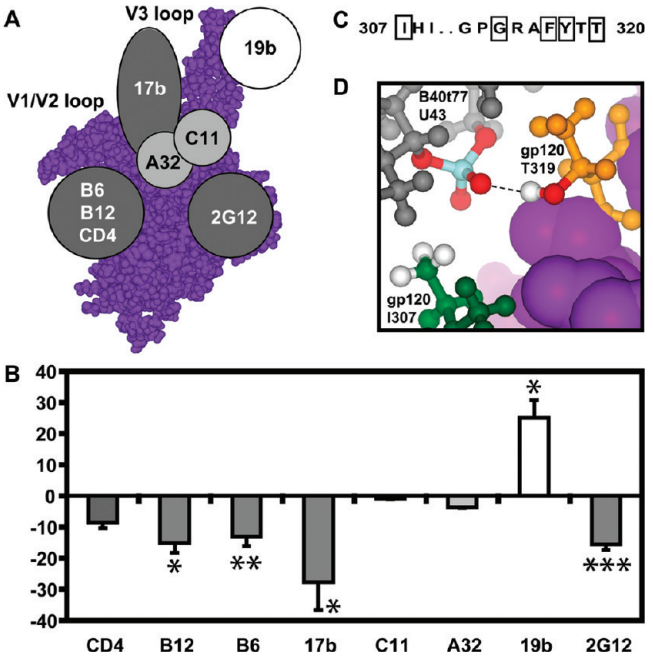

FIGURE 6: B40t77 induced distant conformational changes in gp120. (A) Diagram showing approximate protein binding sites on gp120 (purple). (B) Relative binding responses of antibodies and the CD4 receptor in the presence and absence of B40t77 obtained by SPR. The percent inhibition was calculated as the percent change in binding due to the presence of aptamer. A reduction in the level of binding in the presence of aptamer is shown in dark gray, an increase in the level of binding in white, and no change in light gray. The average of three runs is reported, where error bars represent the percent uncertainty. Proteins whose binding was significantly different in the presence of B40t77 as determined by a *t* test are indicated by asterisks: one for $P < 0.05$, two for $P < 0.01$, and three for $P < 0.001$. (C) Sequence of the HIV-1 gp120 V3 loop bound by the antibody 19b (numbering according to PDB entry 2B4C). Boxes highlight amino acids known to directly participate in the interaction (*42*). (D) Close-up of the modeled interaction of B40t77 and the V3 loop of gp120. I307 (green), an activating mutation, is adjacent to T319 (orange), which was modeled in a position to hydrogen bond with B40t77. B40t77 is colored gray and gp120 purple. Additional atoms are colored red (oxygen), white (hydrogen), and light blue (phosphate). Hydrogen bonds are represented by dotted lines.

binding of 19b to gp120 in the presence of B40t77 indicates that conformational changes with different effects may occur. In support of this, gp120 I307, an amino acid in the V3 loop of gp120 previously predicted to bind 19b (Figure 6C) (*42*), was also the only mutation to cause an increase in the level of binding to B40t77 (Table 1). The B40t77−gp120 model shows that an amino acid in the vicinity of I307, T319, is modeled in a position to hydrogen bond with the B40t77 backbone (Figure 6D). These results suggest that B40t77 may cause neutralization of the virus by inducing distant conformational changes in gp120 that inhibit interaction between gp120 and host receptors, thus disrupting the mechanism of viral entry and host infection.

DISCUSSION

We have used molecular modeling to predict the tertiary structure of a nucleic acid aptamer (B40t77), alone and in complex with gp120. This aptamer is known to specifically interact with gp120 and to potently neutralize a broad range of HIV-1 primary isolates (*21*, *24*). Historically, most simulated docking approaches were developed for the binding of non-nucleic acid ligands to proteins and have yet to be reliably

optimized for nucleic acid research (*34*). For instance, AutoDock was found to have a 50−60% success rate for reproducing experimentally observed RNA complexes (*45*). RNA is a particularly challenging target to model in silico because of the high flexibility, base pairing capability, and presence of bridging water molecules. In this work, previously reported biophysical and biochemical data from the investigation of the interaction of B40t77 with gp120 were used to optimize the model (*21*, *24*, *25*, *29*). By generating a model that agreed with existing experimental data, we hoped to obtain a more physiologically relevant representation of the complex that could be used as a tool to probe the neutralization ability of these aptamers (*46*).

The B40t77 modeled structure displays a Y-like shape with the predicted gp120 binding site in the mouth of the Y, suggesting that B40t77 may function as a molecular clamp that grasps gp120. This clamp may change conformation upon binding as suggested by the comparison of the closed and open tertiary models of B40t77. Docking the closed form of B40t77 onto gp120 generated a complex with an electrostatically favorable and well hydrogen bonded interface. The aptamer-binding site (aptatope) on gp120 was previously predicted to have a smaller footprint on gp120 than other gp120 binding molecules, such as CCR5 or antibodies (*24*, *25*, *29*). The results reported here suggest that the B40t77−gp120 docked complex has a larger, more elongated footprint than previously expected and may extend to the V3 loop. Testing mutations on the edge of the aptatope, such has K117A and Q114A, or on the V3 loop, such as I307A and T319A, enabled us to define the extent of the footprint beyond the previously published data.

To validate the docked model, site-directed mutagenesis targeted against the predicted B40t77−gp120 interface was employed. In summary, 10 gp120 mutants were destabilizing, three showed no change, and one was activating (Table 1). Differences in binding for the destabilizing and activating mutations were found to be statistically significant ($P < 0.05$). Four amino acids of gp120 (Q114, K117, K207, and I439) that weakened binding to B40t77 by at least 10-fold when mutated to alanine are naturally conserved among all HIV-1 isolates (*13*). This suggests that B40t77 may make direct contact with at least four conserved core residues on gp120 within the CCR5-binding site, which the virus cannot afford to mutate without losing fitness or selective advantage.

Recent data have shown that 10 gp120 point mutations (K121A, P299A, N301A, N302A, A329K, N339A, D368A, I420A, W427A, and Y435A), which are predicted to be outside of the B40t77−gp120 interface according to the model, did not significantly reduce the level of binding to a roughly 50-nucleotide, synthetic, and 5′-biotinylated derivative of B40t77, called 299.5 (shown to have binding affinity at least at the level of that of B40t77) (*29*). The location of 10 destabilizing mutations in the predicted B40t77−gp120 interface as shown in Figure 3E, and an additional set outside the interface that showed no effect on aptamer binding (*29*), provides further support for the model. In contrast to our results, the 299.5 aptamer showed a significant reduction in the level of binding to gp120 for two mutations located in the predicted interface, K421A ($P < 0.05$) and I423A ($P < 0.001$). This suggests that biotinylation and/or truncation of B40t77 may slightly alter the folding of the aptamer and hence decrease the affinity of the interaction with gp120 at these positions. Although the possibility that gp120 mutations outside the interface could disrupt aptamer binding though local conformational changes or electrostatic effects cannot be entirely excluded, this seems unlikely given that the overall integrity of gp120 was maintained (demonstrated by the efficient binding of gp120 to antibody C11) and that noninterface mutations (including those that are charged) do not disrupt binding.

A preliminary test showed that B40t77 migrates on a native agarose gel consistent with a monomer and thus might be visualized as a 1:1 complex with gp120. The presence of higher-order aggregates of the molecule after freezing and thawing indicates that it may exist in solution in the monomeric state and may be sensitive to unfolding and aggregation upon mild stress treatment. However, the use of more sophisticated techniques in the future that examine the oligomeric state of the aptamer will also be crucial to defining its conformational stability. Electron microscopy revealed that the dimensions of the B40t77−gp120 complex compared to gp120 alone were consistent with the model, and statistically significant ($P < 0.0001$). Specifically, only the longest axis of the B40t77−gp120 complex (123 ± 16 Å) increased in length when compared to that of gp120 alone (94 ± 10 Å). These results indicate that B40t77 may exist in the monomeric state in solution, may bind to gp120 in a 1:1 complex, and may interact with gp120 in a manner consistent with the model.

The ability of B40t77 to induce distant conformational changes in gp120 was demonstrated by the weakened binding of proteins to gp120 in the presence of aptamer. B40t77 was found to significantly reduce the level of binding of gp120 to monoclonal antibodies B6, B12, and 2G12. The level of binding to the CD4 receptor was also reduced, although the difference was not found to be statistically significant. None of these gp120 binding proteins are predicted to be sterically inhibited by the presence of B40t77. However, nonspecific binding between B40t77 and gp120 that is partially responsible for the reduction in the level of antibody binding cannot be entirely excluded. The binding of the CD4 receptor to its binding site on gp120 has previously been shown to induce distant changes in conformation that increase the level of binding of antibody 17b to the CCR5 binding site (*47*). Therefore, the opposite also seems plausible, that binding of B40t77 to the CCR5 binding site of gp120 could induce distant conformational changes that affect remote sites, consistent with the results reported here.

Antibody 19b showed an increase in the level of binding in the presence of B40t77, perhaps indicating that conformational changes in gp120 can lead to activation. The enhanced binding of 19b may be due to conformational changes in the V3 loop induced by B40t77 resulting in increased exposure of the 19b epitope, which was thought to occur with other gp120 antibodies that bind synergistically (*48*). In support of this, the only activating mutation, gp120 I307A, is also located in the V3 loop and may indicate that this is a flexible region of the molecule susceptible to conformational changes. Consistent with the modeling presented here, I307A may cause a conformational change in the V3 loop that permits stronger hydrogen bonding between B40t77 and T319, an adjacent amino acid that is modeled to hydrogen bond to B40t77 (Figure 6D).

These results, combined with previous evidence (*21*, *24*, *25*, *29*), suggest that the B40t77 binding site overlaps with the CCR5 binding site on gp120 and may explain the ability of B40t77 to inhibit a broad range of clinical isolates (*21*). A previously docked model of the CCR5 N-terminus and a crystal structure of gp120 showed that CCR5 interacts with specific residues at the base of the V3 loop (*38*). Five gp120 residues in the CCR5−gp120 docked interface, R298, D325, R327, I439, and R440 (*38*), were also found to destabilize the interaction of gp120 with B40t77

when mutated to alanine in our system. This includes our most destabilizing mutation, D325A, located at the base of the V3 loop (Figure 3E), and modeled as being in a position to hydrogen bond with B40t77 (Figure 4B). The modeling of the B40t77 binding site to a core part of the coreceptor binding site may provide a partial explanation for the antiviral activity of B40t77.

Overall, the neutralization ability of B40t77 appears to be due to a combination of steric inhibition of CCR5 binding to gp120 and distant conformational changes upon binding that prevent the interaction of gp120 with host cells. Aptamers have the potential to be used as molecular tools to investigate the HIV-1 entry process and subsequent conformational changes. Future experiments that investigate the interaction of B40t77 and gp120 and subsequent conformational changes in an in vitro cellular system should provide new insights into the mechanism of HIV-1 infectivity.

ACKNOWLEDGMENT

We thank Lynn Morris and Elin Gray of the National Institute for Communicable Diseases for antibodies, Dr. William James of Oxford for providing the B40 clone and for insightful comments, the National Institutes of Health AIDS Research and Reference Reagent Program for donating gp120 and antibodies, and Walter Campos, Lia Rotherham, and Dayaneethie Coopusamy for discussions and advice.

REFERENCES

1. Coovadia, H. M., and Hadingham, J. (2005) HIV/AIDS: Global trends, global funds and delivery bottlenecks. *Global Health 1*, 13.
2. Garrib, A., Jaffar, S., Knight, S., Bradshaw, D., and Bennish, M. L. (2006) Rates and causes of child mortality in an area of high HIV prevalence in rural South Africa. *Trop. Med. Int. Health 11*, 1841–1848.
3. UNAIDS/WHO (2008).
4. Schreiber, M., Muller, H., Wachsmuth, C., Laue, T., Hufert, F. T., Van Laer, M. D., and Schmitz, H. (1997) Escape of HIV-1 is associated with lack of V3 domain-specific antibodies in vivo. *Clin. Exp. Immunol. 107*, 15–20.
5. McCutchan, F. E. (2006) Global epidemiology of HIV. *J. Med. Virol. 78* (Suppl. 1), S7–S12.
6. Williamson, C., Morris, L., Maughan, M. F., Ping, L. H., Dryga, S. A., Thomas, R., Reap, E. A., Cilliers, T., van Harmelen, J., Pascual, A., Ramjee, G., Gray, G., Johnston, R., Karim, S. A., and Swanstrom, R. (2003) Characterization and selection of HIV-1 subtype C isolates for use in vaccine development. *AIDS Res. Hum. Retroviruses 19*, 133–144.
7. Gray, E. S., Meyers, T., Gray, G., Montefiori, D. C., and Morris, L. (2006) Insensitivity of paediatric HIV-1 subtype C viruses to broadly neutralising monoclonal antibodies raised against subtype B. *PLoS Med. 3*, e255.
8. Lackner, A. A., and Veazey, R. S. (2007) Current concepts in AIDS pathogenesis: Insights from the SIV/macaque model. *Annu. Rev. Med. 58*, 461–476.
9. Tsibris, A. M., and Kuritzkes, D. R. (2007) Chemokine antagonists as therapeutics: Focus on HIV-1. *Annu. Rev. Med. 58*, 445–459.
10. Srivastava, I. K., Stamatatos, L., Kan, C. E., Vajdy, M., Lian, Y., Hilt, S., Martin, L., Vita, C., Zhu, P., Roux, K. H., Vojtech, L., C Montefiori, D., Donnelly, J., Ulmer, J. B., and Barnett, S. W. (2003) Purification, characterization, and immunogenicity of a soluble trimeric envelope protein containing a partial deletion of the V2 loop derived from SF162, an R5-tropic human immunodeficiency virus type 1 isolate. *J. Virol. 77*, 11244–11259.
11. Yang, X., Florin, L., Farzan, M., Kolchinsky, P., Kwong, P. D., Sodroski, J., and Wyatt, R. (2000) Modifications that stabilize human immunodeficiency virus envelope glycoprotein trimers in solution. *J. Virol. 74*, 4746–4754.
12. Wyatt, R., and Sodroski, J. (1998) The HIV-1 envelope glycoproteins: Fusogens, antigens, and immunogens. *Science 280*, 1884–1888.
13. Kwong, P. D., Wyatt, R., Robinson, J., Sweet, R. W., Sodroski, J., and Hendrickson, W. A. (1998) Structure of an HIV gp120 envelope glycoprotein in complex with the CD4 receptor and a neutralizing human antibody. *Nature 393*, 648–659.
14. Sharon, M., Gorlach, M., Levy, R., Hayek, Y., and Anglister, J. (2002) Expression, purification, and isotope labeling of a gp120 V3 peptide and production of a Fab from a HIV-1 neutralizing antibody for NMR studies. *Protein Expression Purif. 24*, 374–383.
15. Huang, C. C., Tang, M., Zhang, M. Y., Majeed, S., Montabana, E., Stanfield, R. L., Dimitrov, D. S., Korber, B., Sodroski, J., Wilson, I. A., Wyatt, R., and Kwong, P. D. (2005) Structure of a V3-containing HIV-1 gp120 core. *Science 310*, 1025–1028.
16. Bunka, D. H., and Stockley, P. G. (2006) Aptamers come of age—at last. *Nat. Rev. Microbiol. 4*, 588–596.
17. Cerchia, L., Hamm, J., Libri, D., Tavitian, B., and de Franciscis, V. (2002) Nucleic acid aptamers in cancer medicine. *FEBS Lett. 528*, 12–16.
18. Chen, F., Zhou, J., Luo, F., Mohammed, A. B., and Zhang, X. L. (2007) Aptamer from whole-bacterium SELEX as new therapeutic reagent against virulent *Mycobacterium tuberculosis*. *Biochem. Biophys. Res. Commun. 357*, 743–748.
19. Lee, J. F., Stovall, G. M., and Ellington, A. D. (2006) Aptamer therapeutics advance. *Curr. Opin. Chem. Biol. 10*, 282–289.
20. Ng, E. W., Shima, D. T., Calias, P., Cunningham, E. T., Jr., Guyer, D. R., and Adamis, A. P. (2006) Pegaptanib, a targeted anti-VEGF aptamer for ocular vascular disease. *Nat. Rev. Drug Discovery 5*, 123–132.
21. Khati, M., Schuman, M., Ibrahim, J., Sattentau, Q., Gordon, S., and James, W. (2003) Neutralization of infectivity of diverse R5 clinical isolates of human immunodeficiency virus type 1 by gp120-binding 2′F-RNA aptamers. *J. Virol. 77*, 12692–12698.
22. Held, D. M., Kissel, J. D., Patterson, J. T., Nickens, D. G., and Burke, D. H. (2006) HIV-1 inactivation by nucleic acid aptamers. *Front. Biosci. 11*, 89–112.
23. Kwong, P. D., Doyle, M. L., Casper, D. J., Cicala, C., Leavitt, S. A., Majeed, S., Steenbeke, T. D., Venturi, M., Chaiken, I., Fung, M., Katinger, H., Parren, P. W., Robinson, J., Van Ryk, D., Wang, L., Burton, D. R., Freire, E., Wyatt, R., Sodroski, J., Hendrickson, W. A., and Arthos, J. (2002) HIV-1 evades antibody-mediated neutralization through conformational masking of receptor-binding sites. *Nature 420*, 678–682.
24. Dey, A. K., Khati, M., Tang, M., Wyatt, R., Lea, S. M., and James, W. (2005) An aptamer that neutralizes R5 strains of human immunodeficiency virus type 1 blocks gp120-CCR5 interaction. *J. Virol. 79*, 13806–13810.
25. Dey, A. K., Griffiths, C., Lea, S. M., and James, W. (2005) Structural characterization of an anti-gp120 RNA aptamer that neutralizes R5 strains of HIV-1. *RNA 11*, 873–884.
26. Zuker, M. (2003) Mfold web server for nucleic acid folding and hybridization prediction. *Nucleic Acids Res. 31*, 3406–3415.
27. Matzura, O., and Wennborg, A. (1996) RNAdraw: An integrated program for RNA secondary structure calculation and analysis under 32-bit Microsoft Windows. *Comput. Appl. Biosci. 12*, 247–249.
28. Pearce, B. C., Langley, D. R., Kang, J., Huang, H., and Kulkarni, A. (2009) E-novo: An automated workflow for efficient structure-based lead optimization. *J. Chem. Inf. Model. 49*, 1797–1809.
29. Cohen, C., Forzan, M., Sproat, B., Pantophlet, R., McGowan, I., Burton, D., and James, W. (2008) An aptamer that neutralizes R5 strains of HIV-1 binds to core residues of gp120 in the CCR5 binding site. *Virology 381*, 46–54.
30. Darbha, R., Phogat, S., Labrijn, A. F., Shu, Y., Gu, Y., Andrykovitch, M., Zhang, M. Y., Pantophlet, R., Martin, L., Vita, C., Burton, D. R., Dimitrov, D. S., and Ji, X. (2004) Crystal structure of the broadly cross-reactive HIV-1-neutralizing Fab X5 and fine mapping of its epitope. *Biochemistry 43*, 1410–1417.
31. Solomaha, E., Szeto, F. L., Yousef, M. A., and Palfrey, H. C. (2005) Kinetics of Src homology 3 domain association with the proline-rich domain of dynamins: Specificity, occlusion, and the effects of phosphorylation. *J. Biol. Chem. 280*, 23147–23156.
32. Henriksson-Peltola, P., Sehlen, W., and Haggard-Ljungquist, E. (2007) Determination of the DNA-binding kinetics of three related but heteroimmune bacteriophage repressors using EMSA and SPR analysis. *Nucleic Acids Res. 35*, 3181–3191.
33. Karlsson, R., Michaelsson, A., and Mattsson, L. (1991) Kinetic analysis of monoclonal antibody-antigen interactions with a new biosensor based analytical system. *J. Immunol. Methods 145*, 229–240.
34. Moitessier, N., Westhof, E., and Hanessian, S. (2006) Docking of aminoglycosides to hydrated and flexible RNA. *J. Med. Chem. 49*, 1023–1033.
35. Long, S. B., Long, M. B., White, R. R., and Sullenger, B. A. (2008) Crystal structure of an RNA aptamer bound to thrombin. *RNA 14*, 2504–2512.

36. Huang, D. B., Vu, D., Cassiday, L. A., Zimmerman, J. M., Maher, L. J., III, and Ghosh, G. (2003) Crystal structure of NF-κB (p50)2 complexed to a high-affinity RNA aptamer. *Proc. Natl. Acad. Sci. U.S.A. 100*, 9268–9273.
37. Muriaux, D., De Rocquigny, H., Roques, B. P., and Paoletti, J. (1996) NCp7 activates HIV-1Lai RNA dimerization by converting a transient loop-loop complex into a stable dimer. *J. Biol. Chem. 271*, 33686–33692.
38. Huang, C. C., Lam, S. N., Acharya, P., Tang, M., Xiang, S. H., Hussan, S. S., Stanfield, R. L., Robinson, J., Sodroski, J., Wilson, I. A., Wyatt, R., Bewley, C. A., and Kwong, P. D. (2007) Structures of the CCR5 N terminus and of a tyrosine-sulfated antibody with HIV-1 gp120 and CD4. *Science 317*, 1930–1934.
39. Rits-Volloch, S., Frey, G., Harrison, S. C., and Chen, B. (2006) Restraining the conformation of HIV-1 gp120 by removing a flexible loop. *EMBO J. 25*, 5026–5035.
40. Scanlan, C. N., Pantophlet, R., Wormald, M. R., Ollmann Saphire, E., Stanfield, R., Wilson, I. A., Katinger, H., Dwek, R. A., Rudd, P. M., and Burton, D. R. (2002) The broadly neutralizing anti-human immunodeficiency virus type 1 antibody 2G12 recognizes a cluster of α1→2 mannose residues on the outer face of gp120. *J. Virol. 76*, 7306–7321.
41. Wyatt, R., Kwong, P. D., Desjardins, E., Sweet, R. W., Robinson, J., Hendrickson, W. A., and Sodroski, J. G. (1998) The antigenic structure of the HIV gp120 envelope glycoprotein. *Nature 393*, 705–711.
42. Moore, J. P., Trkola, A., Korber, B., Boots, L. J., Kessler, J. A., II, McCutchan, F. E., Mascola, J., Ho, D. D., Robinson, J., and Conley, A. J. (1995) A human monoclonal antibody to a complex epitope in the V3 region of gp120 of human immunodeficiency virus type 1 has broad reactivity within and outside clade B. *J. Virol. 69*, 122–130.
43. Moore, J. P., Willey, R. L., Lewis, G. K., Robinson, J., and Sodroski, J. (1994) Immunological evidence for interactions between the first, second, and fifth conserved domains of the gp120 surface glycoprotein of human immunodeficiency virus type 1. *J. Virol. 68*, 6836–6847.
44. Pantophlet, R., Ollmann Saphire, E., Poignard, P., Parren, P. W., Wilson, I. A., and Burton, D. R. (2003) Fine mapping of the interaction of neutralizing and nonneutralizing monoclonal antibodies with the CD4 binding site of human immunodeficiency virus type 1 gp120. *J. Virol. 77*, 642–658.
45. Detering, C., and Varani, G. (2004) Validation of automated docking programs for docking and database screening against RNA drug targets. *J. Med. Chem. 47*, 4188–4201.
46. Karplus, M., and McCammon, J. A. (2002) Molecular dynamics simulations of biomolecules. *Nat. Struct. Biol. 9*, 646–652.
47. Zhang, W., Canziani, G., Plugariu, C., Wyatt, R., Sodroski, J., Sweet, R., Kwong, P., Hendrickson, W., and Chaiken, I. (1999) Conformational changes of gp120 in epitopes near the CCR5 binding site are induced by CD4 and a CD4 miniprotein mimetic. *Biochemistry 38*, 9405–9416.
48. Cavacini, L., Duval, M., Song, L., Sangster, R., Xiang, S. H., Sodroski, J., and Posner, M. (2003) Conformational changes in env oligomer induced by an antibody dependent on the V3 loop base. *AIDS 17*, 685–689.